Impact of horizontal resolution and model time step on European precipitation extremes in the OpenIFS 43r3 atmosphere model

Yingxue Liu[1,2], Joakim Kjellsson[1,2], Abhishek Savita[1] and Wonsun Park[3,4]

[1]GEOMAR Helmholtz Centre for Ocean Research Kiel, Kiel, Germany

[2]Faculty of Mathematics and Natural Sciences, Christian Albrechts University of Kiel, Kiel, Germany

[3]Center for Climate Physics, Institute for Basic Science (IBS), Busan, Republic of Korea

[4]Department of Climate System, Pusan National University, Busan, Republic of Korea

Correspondence to: Yingxue Liu (yiliu@geomar.de)

Abstract: Events of extreme precipitation pose a hazard to many parts of Europe but are typically not well represented in climate models. Here, we evaluate daily extreme precipitation over Europe during 1982–2019 in observations (GPCC), reanalysis (ERA5) and a set of atmosphere-only simulations at low- (100 km), medium- (50 km) and high- (25 km) horizontal resolution with identical vertical resolutions using OpenIFS (version 43r3). We find that both OpenIFS simulations and reanalysis underestimate the rates of extreme precipitation compared to observations. The biases are largest for the lowest resolution (100 km) and decrease with increasing horizontal resolution (50 and 25 km) simulations in all seasons. The sensitivity to horizontal resolution is particularly high in mountain regions (such as the Alps, Scandinavia, Iberian Peninsula), likely linked to the sensitivity of vertical velocity to the representation of topography. The sensitivity of precipitation to model resolution increases dramatically with increasing percentiles, with modest biases in the 70th–80th percentile range and large biases above the 99th percentile range. We also find that precipitation above the 99th percentile mostly consists of large-scale precipitation (~80 %) in winter, while in summer it is mostly large-scale precipitation in Northern Europe (~70 %) and convective precipitation in Southern Europe (~70 %). Compared to ERA5, the OpenIFS overestimates large-scale precipitation extremes in winter, but underestimates in summer. The discrepancy between OpenIFS and ERA5 decreases with increasing horizontal resolutions. We also examine the sensitivity of extreme precipitation to model time step and find that the convective contribution to extreme precipitation is more sensitive to the model time step than the horizontal resolution. This is likely due to the sensitivity of convective activity to model time step. On the other hand, the large-scale contribution to extreme precipitation is more sensitive to horizontal resolution than the model

time step, which may be due to sharper fronts and steeper topography at higher horizontal resolution.

1. Introduction

Extreme precipitation events have severe impacts on our society and ecosystems. For example, extreme precipitation caused a devastating flood in Germany in 2021, in which around 180 people died. The frequency and intensity of extreme precipitation are projected to increase over most regions in the future (Myhre et al., 2019, Intergovernmental Panel on Climate Change, 2023; Li et al., 2021). The increasing extreme precipitation poses a threat for society and must thus be realistically simulated and projected accurately for future climates. However, the climate models have large biases in simulating extreme precipitation events due to coarse horizontal resolution grid and long model time step etc. (Alexander et al., 2019; Avila et al., 2015; Sillmann et al., 2013). The model biases are also hard to evaluate as we lack long-term observations. This study aims to understand the sensitivity of extreme precipitation to model horizontal resolution and model time step.

Extreme precipitation events are usually underestimated in CMIP models (O'Gorman, 2015; Sillmann et al., 2013). Some studies found the simulated extreme precipitation at higher atmosphere horizontal resolutions is more realistic (Wehner et al., 2010, 2014). Jong et al. (2023) found that the characteristics of extreme precipitation at 25 km resolution configurations have smaller biases that at 50 and 100 km. While, Kopparla et al. (2013) found that the reduced extreme precipitation biases at higher horizontal resolution do not hold for all regions (e.g., Australia).

Strandberg and Lind (2021) reported the effect of horizontal resolution on European extreme precipitation is largest in regions with complex topography and in the summer season when precipitation is mostly caused by convective processes using coupled models, in agreement with Iles et al. (2020). However, Li et al. (2011) demonstrated that the impact of horizontal resolution on global precipitation extremes is manifested mostly by its effects on large-scale precipitation, which could be due to the improved large-scale circulation (Hack et al., 2006). Other studies also found an increasing large-scale precipitation with higher resolution but the convective precipitation is rather insensitive to resolution (Jung et al., 2012; Kopparla et al., 2013; Bacmeister et al., 2013).

No global atmosphere-model simulations explicitly resolve all the physical processes and all must therefore employ parametrizations of such motions. Both the individual physical parameterization and their coupling to the dynamics can benefit from a shorter time step (Jung et al., 2012). Mishra & Sahany (2011) found a more realistic simulation of the heavy precipitation in the tropics when the time step was shortened from 60 min to 5 min at a coarse (~300 km) resolution in a short-period (12 months) configuration. Jung et al. (2012) reported that the biases of mean precipitation were smaller at 60 minutes than at 15 minutes with 126 km resolution in IFS model. However, Roberts et al. (2018) found a minimal impact on model biases when shorten the time step from 20 to 15 minutes at 25 km in IFS model. They either did not investigate the multi-year precipitation extremes, or did not explore the extremes in IFS model.

A recent study by Savita et al. (2024) explored the sensitivity of global mean precipitation to the horizontal resolution and model time step in atmosphere-only simulations with OpenIFS. However, the extreme precipitation's sensitivity to horizontal resolution and time step was not investigated. In this study, we investigated the impact of horizontal resolutions (~100 km, ~50 km, and ~25 km) and model time steps (60 minutes, 30 minutes, and 15 minutes) on daily extreme precipitation using OpenIFS simulations and compare them with observation. We also studied on the convective and large-scale precipitation in all simulations. Precipitation extremes sensitivity to model time step is the first time explored in this work using 100 km in OpenIFS atmosphere model. Besides the extremes, we also explored multi-percentile precipitation's sensitivity to horizontal resolution and time step. This paper is structured as follows: section 2 describes the data and methodology, and section 3 discusses the results. The conclusion and discussion can be found in section 4.

2. Data and Methods

2.1 Model, observation, and reanalysis data

The OpenIFS is derived from the Integrated Forecasting System at the European Centre for Medium-range Weather Forecasting (ECMWF-IFS) cycle 43 release 3 (43r3) (ECMWF, 2017). We use the same AMIP simulations that were used in Savita et al. (2024) which cover the

period 1979-2014 and are extended to 2019 using sea-surface temperature (SST) from ERA5 and the Shared Socioeconomic Pathway 5 (SSP5-8.5) scenario from CMIP6. OpenIFS simulations use 91 vertical levels (L91) and the different horizontal resolutions: low resolution (Tco95, ~100 km), medium resolution (Tco199, ~50 km), and high resolution (Tco399, ~25 km). For the low resolution, additional sensitivity experiments use different model time steps i.e., 60, 30, and 15 minutes and we refer to these experiments as LR60m, LR30m, and LR, respectively. For medium and high resolution, the same model time step is used (i.e., 15 minutes), of which experiments refer to as MR and HR, respectively. While the OpenIFS uses a reduced octahedral grid (Malardel et al., 2016), the final output used in this study has been interpolated to a regular grid using the XIOS output server. The LR, LR30m and LR60m data were interpolated to a global 0.9° grid while the MR and HR data were interpolated to a global 0.45° grid, i.e., we are not investigating extreme precipitation in high resolution simulations in their native grid, which will be investigated in future study. The simulations used here were used by Savita et al. (2024) who found improvements in the surface zonal wind, Rossby wave amplitude and phase speed, weather regime patterns, and surface-air temperature when reducing a model time step from 60 minutes to 30 and 15 minutes in low resolution or increasing the horizontal resolution from 100 km to 50 and 25 km. However, Savita et al. (2024) did not find such improvement in the mean precipitation bias by increasing horizontal resolution or reducing the model time step.

To validate OpenIFS simulations, we use the gridded daily precipitation observational data from Global Precipitation Climatology Centre (GPCC) with resolution of 1° × 1° for the period 1982–2019 (Ziese et al., 2022) as well as the reanalysis data from the ECMWF Reanalysis v5 (ERA5) for 1979–2019 (Hersbach et al., 2023). ERA5 is based on the IFS Cy41r2, with 31 km horizontal resolution and 137 levels (Hersbach et al., 2020). We analyzed total, large-scale, and convective precipitation in this study. The total precipitation (convective plus large-scale precipitation) in the IFS is the accumulated precipitation, comprising of rain and snow, that falls to the Earth's surface, and it is not assimilated in the IFS. The convective precipitation is generated by the convection scheme in the IFS, which represents convection at spatial scales smaller than the grid box. The convection scheme follows Sundqvist (1978), which is also used in the OpenIFS. The large-scale precipitation is generated by the cloud scheme (Khairoutdinov & Kogan, 2000), which represents the formation and dissipation of clouds and large-scale precipitation due to changes in atmospheric quantities (such as pressure, temperature, and moisture) predicted directly by the IFS at spatial scales of the grid box or larger. The

autoconversion/accretion parameterization is a non-linear function of the mass of both liquid cloud and rainwater. The calculation follows Khairoutdinov & Kogan (2000) which is derived from large eddy simulation studies of drizzling stratocumulus clouds, and this scheme is also used in OpenIFS. Several studies have evaluated the performance of ERA5 and found that the total precipitation in ERA5 is performing well over the US (Tarek et al., 2020; Xu et al., 2019). For global precipitation, the mean absolute difference over 50° S–50° N between ERA5 and TRMM/3B43 is 0.58 mm/d; the global-mean correlation with GPCP data is 0.77, which is better compared to ERA-Interim (0.63 mm/d and 0.67) (Hersbach et al., 2020). ERA5 also performs well in polar regions in representing wind, temperature and humidity (Graham et al., 2019; Tetzner et al., 2019; Wang et al., 2019).

Here we analyze daily ERA5 and the OpenIFS data over Europe (30° N–72° N, 10° W–40° E) for the period of 1982–2019 to be consistent with GPCC dataset. For comparison, the ERA5, GPCC, MR, and HR data are remapped to LR (~0.9375° × 0.9375°) using the second-order conservative remapping method. The second-order conservative method includes the gradient across the source cell, which is not included in the first-order conservative method. Therefore, it gives a smoother, more accurate representation of the source field (Jones, 1998).

2.2 Methods

Calculation of q^{th} percentile value

We calculated different percentile values using total precipitation from GPCC, ERA5, and OpenIFS simulations. When we calculated the $\boldsymbol{q}^{\mathbf{th}}$ percentile value, the normalized ranking usually did not match the location of the $\boldsymbol{q}^{\mathbf{th}}$ percentile exactly, which means the $\boldsymbol{q}^{\mathbf{th}}$ lies between two indices. Therefore, we determined the location first, then computed the $\boldsymbol{q}^{\mathbf{th}}$ value by interpolating between the two nearest values based on the location. Here we used the formula below to find the location:

$$j = q*(n-1) \quad (1)$$

$\boldsymbol{n}$ is the length of the sample, $\boldsymbol{q}$ is the desired percentile, $\boldsymbol{j}$ is the location which is the distance from the first value X_1 (X_m are the sorted sample values, $\boldsymbol{m}$=1, 2, …, $\boldsymbol{n}$). Then we took $\boldsymbol{i}$ as the nearest (lower) integer of $\boldsymbol{j}$ to get the $\boldsymbol{q}^{\mathbf{th}}$ value P(q) by interpolating.

$$P(q) = X_i + (X_{i+1} - X_i) * (j-i) \quad (2)$$

There are other methods to determine the location of $\boldsymbol{q}^{\mathbf{th}}$ percentile (Hyndman & Fan, 1996), but here we use the 'linear' one.

The convective contribution to extreme precipitation

To calculate the contribution of convective precipitation to total precipitation for a percentile range, at each grid point we accumulated the convective precipitation on all days when the total precipitation is in that percentile range, then divided it by the accumulated total precipitation on those days to get the fraction of convective precipitation.

Calculation of RMSE values

We used the root-mean-square error (RMSE) referenced to GPCC that measures the performance of ERA5 and OpenIFS simulations:

$$\mathrm{RMSE} = \sqrt{\frac{\sum_{i=1}^{n}(x_{mi}-x_{oi})^2}{n}} \quad (3)$$

x_{mi} is the value at i grid point for ERA5 or OpenIFS simulations, x_{oi} is the value for GPCC, n is the number of land grid points over Europe. Using equation (3), we calculated the RMSE values for different percentile ranges. Smaller RMSE values mean the biases between OpenIFS (or ERA5) and GPCC are smaller i.e., the model simulations and ERA5 are performing better.

Confidence intervals

We calculated the 2.5 to 97.5th confidence intervals (CI) for the RMSE for each percentile with a bootstrap method. For example, to calculate the CI for the RMSE of HR (referenced to GPCC observation), we randomly chose n grid cell pairs from GPCC and HR over European land, then calculated their RMSE (n is the number of total land grid points over Europe). This process was repeated for *2000* times. We took the 2.5th and 97.5th percentiles of the distribution of the 2000 RMSEs as the 95 % CI. If the CI for different simulations do not overlap then we refer that they are significantly different.

3. Results

3.1 Extreme precipitation over Europe

We show the time series of 99th percentile precipitation calculated from all grid points and all days in each year over the period 1982–2019 from GPCC, ERA5, and OpenIFS simulations over Europe (Fig. 1). The ERA5 simulates an inter-annual variability of the 99th percentile precipitation similar to that in GPCC. For example, the peak in 2010 and the low in 1994 are well reproduced in the ERA5. OpenIFS simulations do not reproduce the same inter-annual

variability as in GPCC or ERA5 but LR and HR do reproduce the 95 % significant positive trend observed in GPCC (0.03 mm/d/y, not shown), which are ~0.2 mm/d/y for both LR and HR, and it is not significant for MR. We note that the OpenIFS simulations use observed SST and sea-ice concentrations as boundary conditions, but ozone is taken from a photochemical equilibrium (Cariolle & Teyssèdre, 2007) and aerosol concentrations are taken from Copernicus Atmosphere Monitoring Service (CAMS) monthly climatology. Therefore, we do not expect LR, MR and HR to reproduce trends driven by ozone or aerosols forcing. We also find that both ERA5 and OpenIFS simulations have relatively lower 99th percentile precipitation rates compared to GPCC (Fig. 1). The RMSE for ERA5 (0.36 mm/d) is lower than for OpenIFS simulations which is largest for LR (2.03 mm/d) and decreases with increasing horizontal resolution (i.e., 1.13 mm/d for MR and 0.69 mm/d for HR). Note that Fig. 1 does not contain any spatial information and that a mismatch between model data and observations can be due to the 99th percentile occurring in different regions and/or with different magnitudes. The RMSE analysis suggests that ERA5 and HR are close to GPCC and LR is far from GPCC.

Figure 2a–e shows the spatial distribution of the 99th percentile precipitation over Europe for all days in each season for all years in GPCC, ERA5, and OpenIFS simulations, respectively. In general, the extreme precipitation is very low (~ 2 mm/d) in Northern Africa, which is to be expected since the mean precipitation is only 0.5 mm/d in those regions (Fig. S1). The extreme precipitation exceeds 30 mm/d over mountain areas (e.g., Scandinavian mountains, Alps, and Iberian Peninsula) and the north coast of the Mediterranean but is otherwise lower (~15 mm/d). The spatial distribution of extreme precipitation matches that of the mean precipitation pattern (Fig. S1). The high 99th percentile precipitation near mountains is likely due to the forced ascent of westerly (Scandinavia, Iberian Peninsula, British Isles) and southerly (Alps) winds. The high 99th precipitation in the north of the Mediterranean is likely because of warm and moist southerly winds from the Mediterranean Sea. The ERA5 and OpenIFS simulations overall reproduce the spatial distribution of the 99th percentile precipitation from GPCC. However, the magnitudes are different, particularly over the Scandinavian mountains, the Alps, and central Europe near 50° N (Fig. 2a–e). Figure 2f–i show the regional biases for the 99th percentile precipitation referenced to GPCC. LR mostly underestimates the 99th percentile precipitation in mountainous areas and deserts by more than 25 % (Fig. 2g) and the biases are reduced when horizontal resolution is increased in MR and HR (Fig. 2h–i). We also notice that LR

underestimates the 99th percentile precipitation south of the Alps but overestimates it to the north (Fig. 2 (g)), whereas this bias is negligible in higher-resolution simulations (Fig. 2h–i). This could be because the moist southerly winds do not ascend high enough with LR, therefore there is less precipitation formed on the southern side and more moisture is advected over the mountain. The reduced biases near mountain regions in the higher-resolution simulations are likely because higher resolution has a better representation of topography and vertical velocity. A cross section of the topography and annual-mean vertical velocity at 850 hPa and 62° N (Fig. S2 and S3) highlight that the higher-resolution simulations resolve steeper topography, which leads to more ascent and thus more precipitation.

The 99th percentile precipitation over the Alps is more realistic with higher horizontal resolution compared to lower resolution. However, all simulations as well as ERA5 exhibit a negative bias over northeast Italy and west Slovenia (Fig. 2f–i). By analyzing the EOBS data, we find a similar negative bias as in GPCC, but a positive bias in GPCP (Fig. S8d-k). We notice that the extreme precipitation over Alps (include Slovenia) in GPCP is lower than GPCC and EOBS (Fig. S8a-c), which is likely due to the different data sources and grid methods in different observation datasets (e.g., GPCC and EOBS are gauge-based gridded data on the land, but GPCP data combines microwave and infrared measurements, satellites and rain gauges). We do not know which observation dataset is more realistic, therefore, the cause of the negative bias near Slovenia could be a bias in GPCC or a persistent model bias in the ECMWF-IFS on which both ERA5 and OpenIFS are based. In general, ERA5 has a lower RMSE (2.6 mm/d) for extreme total precipitation than OpenIFS simulations, i.e., ERA5 has overall lower biases than LR (4.0 mm/d) and is similar to MR (3.0 mm/d) and HR (2.9 mm/d).

We next calculate the trend for the annual 99th percentile precipitation over Europe (Fig. S4 & S5) and find that the 99th percentile precipitation has a large positive trend in central Europe and a negative trend to the north of the Alps in GPCC (Fig. S4a). The ERA5 reproduces the pattern of the trend found in GPCC but not significant. However, OpenIFS simulations do not have consistent patterns with GPCC (Fig. S4c–e, Fig. S5c–e), with only LR60m reproducing the large positive trend in central Europe (Fig. S5c). Overall, the trend is largely underestimated over central Europe but overestimated over northern Europe in OpenIFS simulations. We have not found any consistent improvement across the horizontal resolution and model time step.

In addition to the 99th percentile precipitation, we calculate annual total precipitation in different percentile ranges, such as 70th–80th, 80th–90th, 90th–95th, 95th–99th, 99th–99.5th, 99.5th–99.9th and larger than 99.9th (i.e., >99.9th) percentile. We calculate the RMSEs for ERA5 and OpenIFS simulations referenced to GPCC in each range and find that the RMSEs for ERA5 and OpenIFS simulations vary strongly across percentile ranges (Fig. 3). The RMSEs increase exponentially with increasing percentiles, from less than 1 mm/d at the 70th–80th percentile range to ~8 mm/d above the 99.9th percentile range. The largest RMSE is found for LR60m above the 99.9th percentile range which is around 12 mm/d [CI: 11.3–12.8 mm/d]. We also find that the RMSEs decrease with finer horizontal resolution for all percentile ranges. The CI of the RMSEs from LR do not overlap with those from higher horizontal resolutions for any percentile range, i.e., the biases from LR are significantly different from that at higher resolutions and thus clearly sensitive to the horizontal resolution. We also find that the RMSE differences between LR simulation and the higher-resolution simulations as well as ERA5 are larger at higher percentile ranges (>95th) than those at lower percentile ranges (<95th). Thus, we conclude that extreme precipitation is more sensitive to horizontal resolution than precipitation at lower percentile ranges (<95th). ERA5 has the smallest RMSE of all datasets above the 95th percentile ranges, i.e., ERA5 has a better representation of the extreme precipitation than our OpenIFS simulations (Fig 3).

The RMSEs for LR60m, LR30m, and LR are increasing with increasing model time steps. However, the CI of RMSE overlap at all percentile ranges, i.e., the sensitivity of precipitation to the model time step is not statistically significant in the low-resolution configurations. While the model time step may influence precipitation, especially convective precipitation, errors from poorly resolved topography probably have a large impact on the RMSE, which would explain the lack of sensitivity to the model time step.

3.2 Relative roles of convective and large-scale precipitation

Total precipitation is the sum of convective and large-scale precipitation. Convective precipitation is related with not explicitly resolved convective motions. Their scales are smaller than the resolution of the model, therefore need to be parametrized. With increasing resolution, convective precipitation decreases as higher-resolution simulations can resolve smaller scales of vertical motions. On the other hand, large-scale precipitation is likely to originate from large-scale synoptic storms. As horizontal resolution increases, grid cells become smaller and

humidity saturation level is reached faster, thus, large-scale precipitation increases (Hertwig et al., 2015). As we showed in Fig. S7, the large-scale precipitation is more frequent in MR and HR compared to LR when it is higher than 20 mm/d. Higher resolution simulations can produce higher large-scale precipitation better than LR. However, convective precipitation also increases with increasing resolution for convective precipitation higher than 20 mm/d (Fig. S6), but if we only consider the European area-mean values (not shown), the JJA convective precipitation decreases and the large-scale precipitation increases with increasing resolution, which is consistent with Hertwig et al. (2015) result. We find that the convective precipitation is sensitive to time step and the smallest time step has the minimum convective precipitation. The large-scale precipitation is insensitive to time step during JJA and DJF.

We calculate the fractions of convective and large-scale precipitation in total precipitation for days when the total precipitation exceeds the 99th percentile in all model simulations and ERA5 (Fig. 4 & 5). Note that, GPCC does not provide convective and large-scale precipitation separately, therefore we compare our OpenIFS simulations to the ERA5 dataset to assess the effect of resolution and model time step in the model simulations. We note that ERA5 is a reanalysis dataset where precipitation is a parametrized variable, and observations of which are not assimilated over Europe. ERA5 monthly precipitation has a good agreement with GPCC on the land, with correlations above 90 % for most of Europe, and above 70 % for Australia, Asia, and North America (Bell et al., 2021). ERA5 also shows smaller biases for mean precipitation than other reanalysis datasets in the tropics compared to the Global Precipitation Climatology Project (GPCP), with relative biases of 13 % for ERA5, 17 % for MERRA-2 and 36 % for JRA-55 (Hassler & Lauer, 2021). The biases for mean precipitation are found smaller over extra-tropics than the tropics compared to the gauge-based precipitation observations, particularly agreeing well with observations over central Europe and South Asia (Lavers et al., 2022). Moreover, ERA5 can capture the locations and patterns of highest precipitations in observations, but cannot simulate the magnitude (Lavers et al., 2022). We also find that the extreme precipitation over Europe in ERA5 is closer to observations than models (Fig. 1, 2, and 3), therefore, we use ERA5 for the benching mark here although it has some known biases.

The ERA5 data and OpenIFS simulations show that, in DJF, the extreme precipitation is nearly 100 % large-scale precipitation over northern Europe, more than 90 % over central Europe, and more than 70 % over western and southern Europe (Fig. 5a–d). However, in JJA, large-scale precipitation makes up most of the extreme precipitation over northern Europe (>70 %)

while convective precipitation makes up most of the extreme precipitation in the Mediterranean region (>70 %) (Fig. 4a–d). The OpenIFS simulations largely reproduce the pattern of the fraction of convective precipitation found in ERA5, but we note differences in magnitudes (Fig. 4e–g, and Fig. 5e–g)). In JJA, the OpenIFS simulates the contribution of the convective precipitation very close to ERA5 over Scandinavia where the extreme precipitation is mostly large-scale precipitation, but has more convective precipitation for other areas over Europe compared to ERA5 (Fig. 4e–g). The RMSEs from MR (0.10 mm/d [CI: 0.09–0.10 mm/d]) and HR (~0.09 mm/d [CI: 0.09–0.10 mm/d]) are not significantly different, while LR (~0.12 mm/d [CI: 0.12–0.13 mm/d]) is significantly larger than those in MR and HR. In DJF, the OpenIFS has less contribution from convective precipitation than ERA5 except for near-coastal areas (Fig. 5e–f). That is, the contribution from large-scale precipitation is more in OpenIFS than ERA5, and their difference is reduced with higher horizontal resolution, i.e., in MR and HR.

Further, we explore the relative roles of horizontal resolution and time step for the large-scale and convective precipitation at different percentile ranges (Fig. 6). In general, the RMSEs increase with increasing percentiles, but also decrease with increasing horizontal resolution and shorter model time step. The RMSE reduces for higher percentile in higher resolution due to better representation of topography, and in smaller model time step due to enhanced convection. The exceptions are the total precipitation above the 99.5th percentile in JJA where the RMSEs from LR are larger than LR30m (Fig. 6a), and the convective precipitation above the 99th percentile in JJA and DJF where the RMSEs from HR are larger than MR (Fig. 6c & f).

The CI for RMSEs of total precipitation from LR, MR and HR in DJF and JJA do not overlap for all percentile ranges, thus there is a significant sensitivity of the total precipitation to the horizontal resolution, particularly for extreme total precipitation. The exceptions are the total precipitation below the 90th percentile ranges and above the 99.9th percentile range in JJA where the CI for RMSEs in MR and HR overlap (Fig. 6a). However, the sensitivity is not found for the global-mean total precipitation by increasing horizontal resolution (Savita et al., 2024). For the large-scale precipitation in JJA, the CI for RMSEs from LR do not overlap with those from MR and HR at higher percentile ranges (>95th), but overlap at lower percentile ranges (<95th) (Fig. 6b). That is, the large-scale precipitation from the extreme precipitation is sensitive to the horizontal resolution. We note that a reduced RMSE with increasing resolutions at >99th is not found for the convective precipitation in JJA (Fig. 6c), and we conclude that the

horizontal resolution dependence of extreme total precipitation in JJA comes from the large-scale precipitation. For DJF, the large-scale precipitation is sensitive to the horizontal resolution for all percentile ranges, where the CI for RMSEs in LR do not overlap with those from MR and HR (Fig. 6e). The convective precipitation in DJF is also sensitive to the horizontal resolution (Fig. 6f), however there is little convection precipitation in DJF, thus the sensitivity for convective precipitation in DJF is not important. Therefore, the resolution dependence of extreme total precipitation is mostly dominated by the large-scale precipitation in DJF.

For the model time step, the CI for RMSEs of total precipitation from LR60m, LR30m, and LR overlap at all percentile ranges in both JJA and DJF (Fig. 6a & d), i.e., the extreme total precipitation is not sensitive to the model time step in a significant way in the low-resolution simulations. Similarly, the mean total precipitation is also found insensitive to the model time step (Savita et al., 2024). Both the large-scale and convective precipitation are sensitive to the model time step particularly above the 95^{th} percentile ranges in JJA (Fig. 6b & c). The convective precipitation is more sensitive to the model time step than the large-scale precipitation in JJA, but in DJF the sensitivity is found only for the large-scale precipitation (Fig. 6e). Also, the lack of sensitivity for convective precipitation in DJF may be because there is almost no convective precipitation in DJF.

4. Discussion and Conclusion

We have investigated the sensitivity of extreme precipitation across different horizontal resolutions and model time steps in atmosphere-only experiments with the OpenIFS. Comparing extreme precipitation (defined as total daily precipitation at the 99^{th} percentile) from OpenIFS simulations, reanalysis (ERA5), and observation (GPCC), we find that MR and HR mostly better represent the precipitation extremes compared to LR. We also found a more significant sensitivity to the horizontal resolution for the precipitation above the 95^{th} percentile and less sensitivity for lower percentile ranges ($<95^{th}$) (Fig. 3). These OpenIFS-based results are similar to Kopparla et al. (2013), who found that the bias of extreme precipitation in the high-resolution simulation (25 km) is reduced compared to the lower-resolution simulations (100 km and 200 km) over Europe in their atmospheric model, but not for precipitation at lower percentiles (i.e., $<95^{th}$). However, the sensitivity to the horizontal resolution found by Kopparla et al. (2013) was not significant over Europe which is rather different from our results as we have found a significant difference across the horizontal resolutions. In contrast to the extreme

401 precipitation, the bias for global mean precipitation is not decreasing when increasing
402 horizontal resolution from ~200 km to ~100 km or ~50 km in the ECHAM6-AMIP simulations
403 (Hertwig et al., 2015), and also in other GCMs (e.g., OpenIFS, HadGEM1 and HadGEM3)
404 (Demory et al., 2020; Savita et al., 2024; Schiemann et al., 2014). However, Delworth et al.
405 (2012) found an improvement in the global mean precipitation with increasing horizontal
406 resolution in a coupled model (GFDL).
407
408 The improvements due to increasing horizontal resolution for the extreme precipitation are
409 mostly over the mountain areas, consistent with previous studies which found the effect of
410 horizontal resolution being largest in areas with complex topography over Europe and also
411 other regions for mean and extreme precipitation (Demory et al., 2020; Iles et al., 2020;
412 Monerie et al., 2020; Prein et al., 2013; Torma et al., 2015). The sensitivity to the horizontal
413 resolution comes from the large-scale precipitation, which is likely because of the better-
414 resolved topography. However, the convective precipitation in JJA is more sensitive to the
415 model time step than it is to the horizontal resolution, likely because there is an increase in
416 shallow and mid-level convection with a shorter time step in the OpenIFS (Savita et al., 2024),
417 thus we get more convective precipitation.
418
419 In our results, larger improvements are obtained when the horizontal resolution is increased
420 from LR to MR, but relatively smaller improvements from MR to HR. Similar results are also
421 found in Roberts et al. (2018), where the climatological surface biases are relatively insensitive
422 when increasing the atmospheric resolution from ~50 km to ~25 km in the ECMWF-IFS. Jung
423 et al. (2012) also showed that the largest improvements in extratropical cyclones, Euro-Atlantic
424 blocking, tropical mean precipitation, and tropospheric circulation are found when increasing
425 horizontal resolution from 126 km to 39 km with relatively small further changes from 39 km
426 to 16 and to 10 km in ECMWF atmosphere model. Kopparla et al. (2013) and Bacmeister et al.
427 (2014) found much improvement for the mean precipitation and extreme precipitation with the
428 increasing atmospheric resolution from ~200 km to 100 km, but less improvement from ~100
429 km to ~25 km. It is likely due to a lack of tuning with the changing horizontal resolution. The
430 above conclusions are valid over Europe, but maybe not valid for other regions such as the
431 tropics and subtropics, where the extreme precipitation is often triggered by tropical cyclones
432 (Gori et al., 2022; Zhu & Quiring, 2022). The distribution of tropical cyclones intensity and
433 the structure of the most intense storm can be adequately simulated at 16 and 10-km horizontal
434 resolutions, but not at 126 and 39-km resolutions in ECMWF-IFS (Manganello et al., 2011).

Moreover, the choice of observation dataset is a key factor for assessing the impact of the horizontal resolution and model time step on extreme precipitation. Most observation precipitation data are from one of the three categories, gauge-based products, satellite products, and merged satellite-gauge products. Since the satellite products are constructed with satellite microwave and/ or infrared measurements, with/ without gauged-adjusted estimates, differences exist between these products. Besides, the gauge-based products are highly dependent on the choice of stations and interpolation schemes. It is hard to say which product is closer to reality, as different regions may have different observation datasets that suit best for the analysis. In particular, we note that not all products are suitable for extreme analysis. For example, GPCP's main scope is to construct a reliable climate data record and has been developed with a priority of ensuring the long-term stability of data (Adler et al., 2017). Masunaga et al. (2019) found that the frequency of GPCP daily precipitation quickly drops below all other datasets once the precipitation exceeds 30 mm/d. Also, the time series of GPCP extreme precipitation over the ocean exhibits a jump to lower 99^{th} percentiles in late 2008/early 2009 which is not present in all other datasets, coinciding with the change in utilization of SSM/I and SSMIS. The lower 99^{th} precipitation suggests that the GPCP dataset might not be applied to extreme analysis (Masunaga et al., 2019). Therefore, we only use GPCC observation data as the reference to explore the model performance. In Fig. 2f–i the 99^{th} percentile precipitation is largely underestimated in the eastern Alp region by ERA5 and all model simulations. The biases are insensitive to horizontal resolution. It is likely a persistent model bias in the ECMWF-IFS or a bias in GPCC. Analyzing multiple precipitation products instead of relying on a single one may be a good way to reduce these biases.

Code and data variability

The OpenIFS model requires a software license agreement with ECMWF to use it, and OpenIFS's license is easily given free of charge to any academic or research institute. The details of OpenIFS are available at https://confluence.ecmwf.int/display/OIFS/About+OpenIFS (ECMWF, 2018). We used the same simulation that used in Savita et al. (2024) and therefore do not provide the data needed to reproduce the simulations here. All data (runscripts, input data etc) needed to reproduce the simulations can be found in Savita et al. (2024) in code and data variability section. The jupyter notebook scripts used in this study to produce the plots can be found at

https://doi.org/10.5281/zenodo.10887652. The raw model output is available from the authors upon reasonable request. The observation and reanalysis datasets used in this study can be downloaded from GPCC (https://opendata.dwd.de/climate_environment/GPCC/html/fulldata-daily_v2022_doi_download.html, Ziese et al., 2022) and ERA5 (https://cds.climate.copernicus.eu/cdsapp#!/dataset/reanalysis-era5-single-levels?tab=form, Hersbach et al., 2023).

Authors contributions. AS and JK conducted all the OpenIFS simulations. YL did the analysis and writing with substantial contribution from JK, AS and WP.

Competing interests. The contact author has declared that none of the authors has any competing interests.

Acknowledgements. Yingxue Liu is supported by China Scholarship Council (CSC, grant no. 202004910401). Joakim Kjellsson and Abhishek Savita are supported by JPI Climate/Ocean (ROADMAP project, grant no. 01LP2002C). Wonsun Park was supported by IBS (grant no. IBS-R028-D1). We thank the OpenIFS team at ECMWF for the technical support. All the OpenIFS simulations were conducted on the HLRN machine under shk00018 project resources. All the analysis and data storage were conducted on computer clusters at GEOMAR and Kiel University Computing Center (NESH).

Financial support. This research is financially supported by CSC (grant no. 202004910401) and ROADMAP project (grant no. 01LP2002C).

References

Adler, R. F., Gu, G., Sapiano, M., Wang, J. J., & Huffman, G. J. (2017). Global Precipitation: Means, Variations and Trends During the Satellite Era (1979–2014). In *Surveys in Geophysics* (Vol. 38, Issue 4, pp. 679–699). Springer Netherlands. https://doi.org/10.1007/s10712-017-9416-4

Alexander, L. V., Fowler, H. J., Bador, M., Behrangi, A., Donat, M. G., Dunn, R., Funk, C., Goldie, J., Lewis, E., Rogé, M., Seneviratne, S. I., & Venugopal, V. (2019). On the use of indices to study extreme precipitation on sub-daily and daily timescales. *Environmental Research Letters*, *14*(12). https://doi.org/10.1088/1748-9326/ab51b6

Avila, F. B., Dong, S., Menang, K. P., Rajczak, J., Renom, M., Donat, M. G., & Alexander, L. V. (2015). Systematic investigation of gridding-related scaling effects on annual statistics of daily temperature and precipitation maxima: A case study for south-east Australia. *Weather and Climate Extremes*, *9*, 6–16. https://doi.org/10.1016/j.wace.2015.06.003

Bacmeister, J. T., Wehner, M. F., Neale, R. B., Gettelman, A., Hannay, C., Lauritzen, P. H., Caron, J. M., & Truesdale, J. E. (2014). Exploratory high-resolution climate simulations using the community atmosphere model (CAM). *Journal of Climate*, *27*(9), 3073–3099. https://doi.org/10.1175/JCLI-D-13-00387.1

Bador, M., Boé, J., Terray, L., Alexander, L. V., Baker, A., Bellucci, A., Haarsma, R., Koenigk, T., Moine, M. P., Lohmann, K., Putrasahan, D. A., Roberts, C., Roberts, M., Scoccimarro, E., Schiemann, R., Seddon, J., Senan, R., Valcke, S., & Vanniere, B. (2020). Impact of Higher Spatial Atmospheric Resolution on Precipitation Extremes Over Land in Global Climate Models. *Journal of Geophysical Research: Atmospheres*, *125*(13). https://doi.org/10.1029/2019JD032184

Barrett, A. I., Wellmann, C., Seifert, A., Hoose, C., Vogel, B., & Kunz, M. (2019). One Step at a Time: How Model Time Step Significantly Affects Convection-Permitting Simulations. *Journal of Advances in Modeling Earth Systems*, *11*(3), 641–658. https://doi.org/10.1029/2018MS001418

Bell, B., Hersbach, H., Simmons, A., Berrisford, P., Dahlgren, P., Horányi, A., Muñoz-Sabater, J., Nicolas, J., Radu, R., Schepers, D., Soci, C., Villaume, S., Bidlot, J. R., Haimberger, L., Woollen, J., Buontempo, C., & Thépaut, J. N. (2021). The ERA5 global reanalysis: Preliminary extension to 1950. *Quarterly Journal of the Royal Meteorological Society*, *147*(741), 4186–4227. https://doi.org/10.1002/qj.4174

Caldwell, P. (2010). California wintertime precipitation bias in regional and global climate models. *Journal of Applied Meteorology and Climatology*, *49*(10), 2147–2158. https://doi.org/10.1175/2010JAMC2388.1

Cariolle, D., & Teyssèdre, H. (2007). Atmospheric Chemistry and Physics A revised linear ozone photochemistry parameterization for use in transport and general circulation models: multi-annual simulations. In *Atmos. Chem. Phys* (Vol. 7). www.atmos-chem-phys.net/7/2183/2007/

Chan, S. C., Kendon, E. J., Fowler, H. J., Blenkinsop, S., Ferro, C. A. T., & Stephenson, D. B. (2013). Does increasing the spatial resolution of a regional climate model improve the simulated daily precipitation? *Climate Dynamics*, *41*(5–6), 1475–1495. https://doi.org/10.1007/s00382-012-1568-9

Delworth, T. L., Rosati, A., Anderson, W., Adcroft, A. J., Balaji, V., Benson, R., Dixon, K., Griffies, S. M., Lee, H. C., Pacanowski, R. C., Vecchi, G. A., Wittenberg, A. T., Zeng, F., & Zhang, R. (2012). Simulated climate and climate change in the

GFDL CM2.5 high-resolution coupled climate model. *Journal of Climate*, *25*(8), 2755–2781. https://doi.org/10.1175/JCLI-D-11-00316.1

Demory, M. E., Berthou, S., Fernández, J., Sørland, S. L., Brogli, R., Roberts, M. J., Beyerle, U., Seddon, J., Haarsma, R., Schär, C., Buonomo, E., Christensen, O. B., Ciarlo, J. M., Fealy, R., Nikulin, G., Peano, D., Putrasahan, D., Roberts, C. D., Senan, R., … Vautard, R. (2020). European daily precipitation according to EURO-CORDEX regional climate models (RCMs) and high-resolution global climate models (GCMs) from the High-Resolution Model Intercomparison Project (HighResMIP). *Geoscientific Model Development*, *13*(11), 5485–5506. https://doi.org/10.5194/gmd-13-5485-2020

Gori, A., Lin, N., Xi, D., & Emanuel, K. (2022). Tropical cyclone climatology change greatly exacerbates US extreme rainfall–surge hazard. *Nature Climate Change*, *12*(2), 171–178. https://doi.org/10.1038/s41558-021-01272-7

Graham, R. M., Hudson, S. R., & Maturilli, M. (2019). Improved Performance of ERA5 in Arctic Gateway Relative to Four Global Atmospheric Reanalyses. *Geophysical Research Letters*, *46*(11), 6138–6147. https://doi.org/10.1029/2019GL082781

Hassler, B., & Lauer, A. (2021). Comparison of reanalysis and observational precipitation datasets including era5 and wfde5. *Atmosphere*, *12*(11). https://doi.org/10.3390/atmos12111462

Hersbach, H., Bell, B., Berrisford, P., Hirahara, S., Horányi, A., Muñoz-Sabater, J., Nicolas, J., Peubey, C., Radu, R., Schepers, D., Simmons, A., Soci, C., Abdalla, S., Abellan, X., Balsamo, G., Bechtold, P., Biavati, G., Bidlot, J., Bonavita, M., … Thépaut, J. N. (2020). The ERA5 global reanalysis. *Quarterly Journal of the Royal Meteorological Society*, *146*(730), 1999–2049. https://doi.org/10.1002/qj.3803

Hertwig, E., von Storch, J. S., Handorf, D., Dethloff, K., Fast, I., & Krismer, T. (2015). Effect of horizontal resolution on ECHAM6-AMIP performance. *Climate Dynamics*, *45*(1–2), 185–211. https://doi.org/10.1007/s00382-014-2396-x

Hyndman, R. J., & Fan, Y. (1996). Sample Quantiles in Statistical Packages. In *Source: The American Statistician* (Vol. 50, Issue 4).

Iles, C. E., Vautard, R., Strachan, J., Joussaume, S., Eggen, B. R., & Hewitt, C. D. (2020). The benefits of increasing resolution in global and regional climate simulations for European climate extremes. *Geoscientific Model Development*, *13*(11), 5583–5607. https://doi.org/10.5194/gmd-13-5583-2020

Intergovernmental Panel on Climate Change. (2023). Weather and Climate Extreme Events in a Changing Climate. In *Climate Change 2021 – The Physical Science Basis* (pp. 1513–1766). Cambridge University Press. https://doi.org/10.1017/9781009157896.013

Jones, P. W. (1998). *First-and Second-Order Conservative Remapping Schemes for Grids in Spherical Coordinates*.

Jong, B. T., Delworth, T. L., Cooke, W. F., Tseng, K. C., & Murakami, H. (2023). Increases in extreme precipitation over the Northeast United States using high-resolution climate model simulations. *Npj Climate and Atmospheric Science*, *6*(1). https://doi.org/10.1038/s41612-023-00347-w

Jung, T., Miller, M. J., Palmer, T. N., Towers, P., Wedi, N., Achuthavarier, D., Adams, J. M., Altshuler, E. L., Cash, B. A., Kinter, J. L., Marx, L., Stan, C., & Hodges, K. I. (2012). High-resolution global climate simulations with the ECMWF model in project athena: Experimental design, model climate, and seasonal forecast skill. *Journal of Climate*, *25*(9), 3155–3172. https://doi.org/10.1175/JCLI-D-11-00265.1

Khairoutdinov, M., & Kogan, Y. (2000). *A New Cloud Physics Parameterization in a Large-Eddy Simulation Model of Marine Stratocumulus*.

Kopparla, P., Fischer, E. M., Hannay, C., & Knutti, R. (2013). Improved simulation of extreme precipitation in a high-resolution atmosphere model. *Geophysical Research Letters*, *40*(21), 5803–5808. https://doi.org/10.1002/2013GL057866

Laprise, R. (2008). Regional climate modelling. *Journal of Computational Physics*, *227*(7), 3641–3666. https://doi.org/10.1016/j.jcp.2006.10.024

Lavers, D. A., Simmons, A., Vamborg, F., & Rodwell, M. J. (2022). An evaluation of ERA5 precipitation for climate monitoring. *Quarterly Journal of the Royal Meteorological Society*, *148*(748), 3152–3165. https://doi.org/10.1002/qj.4351

Li, C., Zwiers, F., Zhang, X., Li, G., Sun, Y., & Wehner, M. (2021). Changes in Annual Extremes of Daily Temperature and Precipitation in CMIP6 Models. *Journal of Climate*, *34*, 3441–3460. https://doi.org/10.1175/JCLI-D-19

Malardel, S., Wedi, N., Deconinck, W., & Kühnlein, C. (2016). *A new grid for the IFS*. https://www.researchgate.net/publication/297695132

Manganello, J. V., Hodges, K. I., Kinter, J. L., Cash, B. A., Marx, L., Jung, T., Achuthavarier, D., Adams, J. M., Altshuler, E. L., Huang, B., Jin, E. K., Stan, C., Towers, P., & Wedi, N. (2012). Tropical cyclone climatology in a 10-km global atmospheric GCM: Toward weather-resolving climate modeling. Journal of Climate, 25(11), 3867–3893. https://doi.org/10.1175/JCLI-D-11-00346.1

Masunaga, H., Schröder, M., Furuzawa, F. A., Kummerow, C., Rustemeier, E., & Schneider, U. (2019). Inter-product biases in global precipitation extremes. *Environmental Research Letters*, *14*(12). https://doi.org/10.1088/1748-9326/ab5da9

Mishra, S. K., & Sahany, S. (2011). Effects of time step size on the simulation of tropical climate in NCAR-CAM3. *Climate Dynamics*, *37*(3), 689–704. https://doi.org/10.1007/s00382-011-0994-4

Monerie, P. A., Chevuturi, A., Cook, P., Klingaman, N. P., & Holloway, C. E. (2020). Role of atmospheric horizontal resolution in simulating tropical and subtropical South American precipitation in HadGEM3-GC31. *Geoscientific Model Development*, *13*(10), 4749–4771. https://doi.org/10.5194/gmd-13-4749-2020

Myhre, G., Alterskjær, K., Stjern, C. W., Hodnebrog, Marelle, L., Samset, B. H., Sillmann, J., Schaller, N., Fischer, E., Schulz, M., & Stohl, A. (2019). Frequency of extreme precipitation increases extensively with event rareness under global warming. *Scientific Reports*, *9*(1). https://doi.org/10.1038/s41598-019-52277-4

O'Gorman, P. A. (2015). Precipitation Extremes Under Climate Change. In *Current Climate Change Reports* (Vol. 1, Issue 2, pp. 49–59). Springer. https://doi.org/10.1007/s40641-015-0009-3

Prein, A. F., Gobiet, A., Suklitsch, M., Truhetz, H., Awan, N. K., Keuler, K., & Georgievski, G. (2013). Added value of convection permitting seasonal simulations. *Climate Dynamics*, *41*(9–10), 2655–2677. https://doi.org/10.1007/s00382-013-1744-6

Rauscher, S. A., O'Brien, T. A., Piani, C., Coppola, E., Giorgi, F., Collins, W. D., & Lawston, P. M. (2016). A multimodel intercomparison of resolution effects on precipitation: simulations and theory. *Climate Dynamics*, *47*(7–8), 2205–2218. https://doi.org/10.1007/s00382-015-2959-5

Savita, A., Kjellsson, J., Kedzierski, R. P., Latif, M., Rahm, T., Wahl, S., & Park, W. (2024). Assessment of climate biases in OpenIFS version 43r3 across model horizontal resolutions and time steps. *Geoscientific Model Development*, *17*(4), 1813–1829. https://doi.org/10.5194/gmd-17-1813-2024

Schiemann, R., Demory, M. E., Mizielinski, M. S., Roberts, M. J., Shaffrey, L. C., Strachan, J., & Vidale, P. L. (2014). The sensitivity of the tropical circulation and

Maritime Continent precipitation to climate model resolution. *Climate Dynamics*, *42*(9–10), 2455–2468. https://doi.org/10.1007/s00382-013-1997-0

Sillmann, J., Kharin, V. V., Zhang, X., Zwiers, F. W., & Bronaugh, D. (2013). Climate extremes indices in the CMIP5 multimodel ensemble: Part 1. Model evaluation in the present climate. *Journal of Geophysical Research Atmospheres*, *118*(4), 1716–1733. https://doi.org/10.1002/jgrd.50203

Strandberg, G., & Lind, P. (2021). The importance of horizontal model resolution on simulated precipitation in Europe – from global to regional models. *Weather and Climate Dynamics*, *2*(1), 181–204. https://doi.org/10.5194/wcd-2-181-2021

Sundqvist, H. (1978). A parameterization scheme for non-convective condensation including prediction of cloud water content. *Quarterly Journal of the Royal Meteorological Society*, *104*(441), 677–690. https://doi.org/10.1002/qj.49710444110

Tarek, M., Brissette, F. P., & Arsenault, R. (2020). Evaluation of the ERA5 reanalysis as a potential reference dataset for hydrological modelling over North America. *Hydrology and Earth System Sciences*, *24*(5), 2527–2544. https://doi.org/10.5194/hess-24-2527-2020

Tetzner, D., Thomas, E., & Allen, C. (2019). A validation of ERA5 reanalysis data in the southern antarctic peninsula—Ellsworth land region, and its implications for ice core studies. *Geosciences (Switzerland)*, *9*(7). https://doi.org/10.3390/geosciences9070289

Torma, C., Giorgi, F., & Coppola, E. (2015). Added value of regional climate modeling over areas characterized by complex terrain-precipitation over the Alps. *Journal of Geophysical Research*, *120*(9), 3957–3972. https://doi.org/10.1002/2014JD022781

Wan, H., Zhang, S., Rasch, P. J., Larson, V. E., Zeng, X., & Yan, H. (2021). Quantifying and attributing time step sensitivities in present-day climate simulations conducted with EAMv1. *Geoscientific Model Development*, *14*(4), 1921–1948. https://doi.org/10.5194/gmd-14-1921-2021

Wang, C., Graham, R. M., Wang, K., Gerland, S., & Granskog, M. A. (2019). Comparison of ERA5 and ERA-Interim near-surface air temperature, snowfall and precipitation over Arctic sea ice: effects on sea ice thermodynamics and evolution. *Cryosphere*, *13*(6), 1661–1679. https://doi.org/10.5194/tc-13-1661-2019

Wehner, M. F., Reed, K. A., Li, F., Prabhat, Bacmeister, J., Chen, C. T., Paciorek, C., Gleckler, P. J., Sperber, K. R., Collins, W. D., Gettelman, A., & Jablonowski, C. (2014). The effect of horizontal resolution on simulation quality in the Community Atmospheric Model, CAM5.1. *Journal of Advances in Modeling Earth Systems*, *6*(4), 980–997. https://doi.org/10.1002/2013MS000276

Wehner, M. F., Smith, R. L., Bala, G., & Duffy, P. (2010). The effect of horizontal resolution on simulation of very extreme US precipitation events in a global atmosphere model. *Climate Dynamics*, *34*(2), 241–247. https://doi.org/10.1007/s00382-009-0656-y

Xu, X., Frey, S. K., Boluwade, A., Erler, A. R., Khader, O., Lapen, D. R., & Sudicky, E. (2019). Evaluation of variability among different precipitation products in the Northern Great Plains. *Journal of Hydrology: Regional Studies*, *24*. https://doi.org/10.1016/j.ejrh.2019.100608

Zhu, L., & Quiring, S. M. (2022). Exposure to precipitation from tropical cyclones has increased over the continental United States from 1948 to 2019. *Communications Earth and Environment*, *3*(1). https://doi.org/10.1038/s43247-022-00639-8

Figures

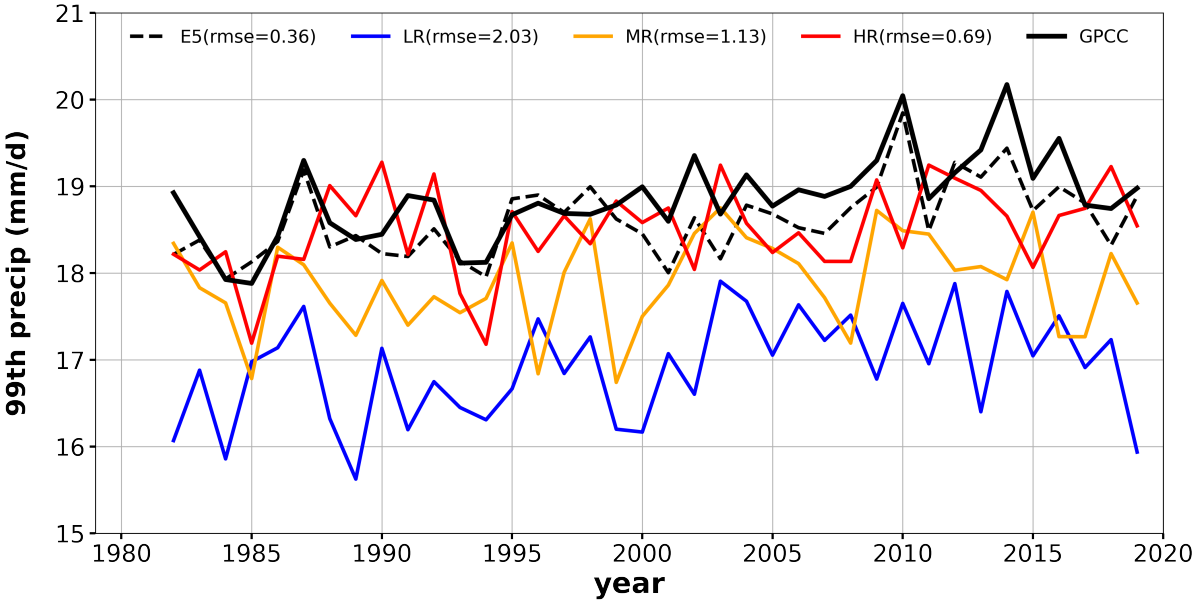

Fig. 1 Annual time series of the 99th percentile precipitation using observations (GPCC, green), reanalysis (ERA5, black), and model simulations (LR: blue, MR: orange, HR: red) during 1982-2019 over Europe. RMSE values of 99th percentile precipitation are computed referenced to GPCC which are shown within the small bracket.

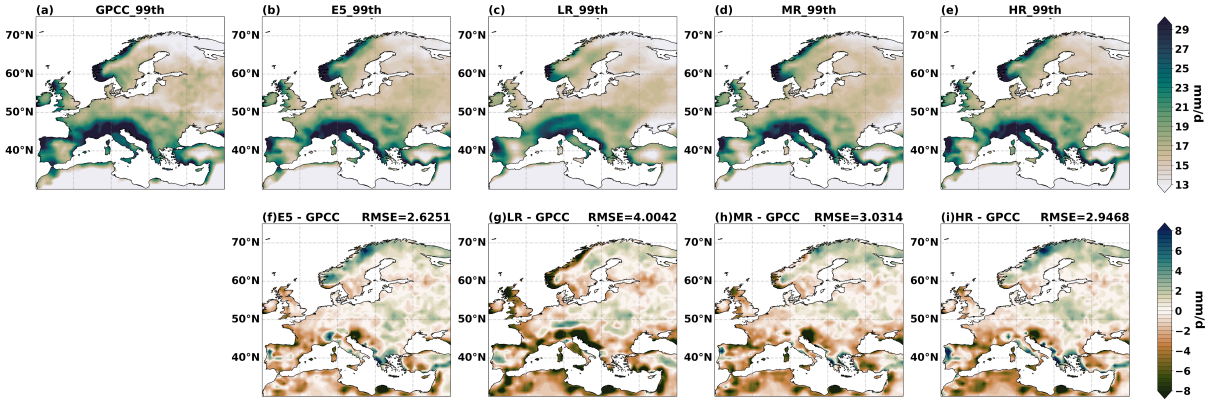

Fig. 2 The 99th percentile precipitation over Europe during 1982-2019 from (a) GPCC observations, (b) ERA5 reanalysis, (c) LR, (d) MR, (e) HR, and the corresponding biases and RMSEs in (f) ERA5, (g) LR, (h) MR, and (i) HR.

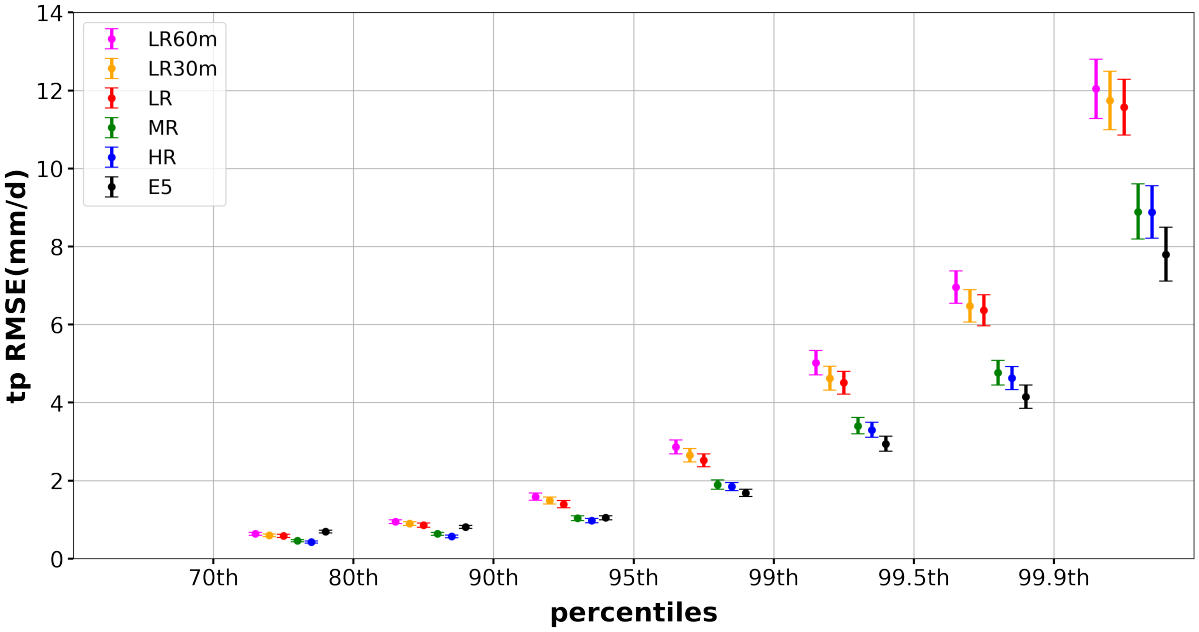

Fig. 3 RMSEs for annual total precipitation at different percentile ranges (70^{th} – 80^{th}, 80^{th} – 90^{th}, 90^{th} – 95^{th}, 95^{th} – 99^{th}, 99^{th} – 99.5^{th}, 99.5^{th} – 99.9^{th} and >99.9^{th} percentile) in ERA5 (black) and OpenIFS simulations (LR60m: magenta, LR30m: orange, LR: red, MR: green, HR: blue) referenced to GPCC during 1982-2019 over Europe. Dots are the RMSE values, and error bars are the 95 % CI.

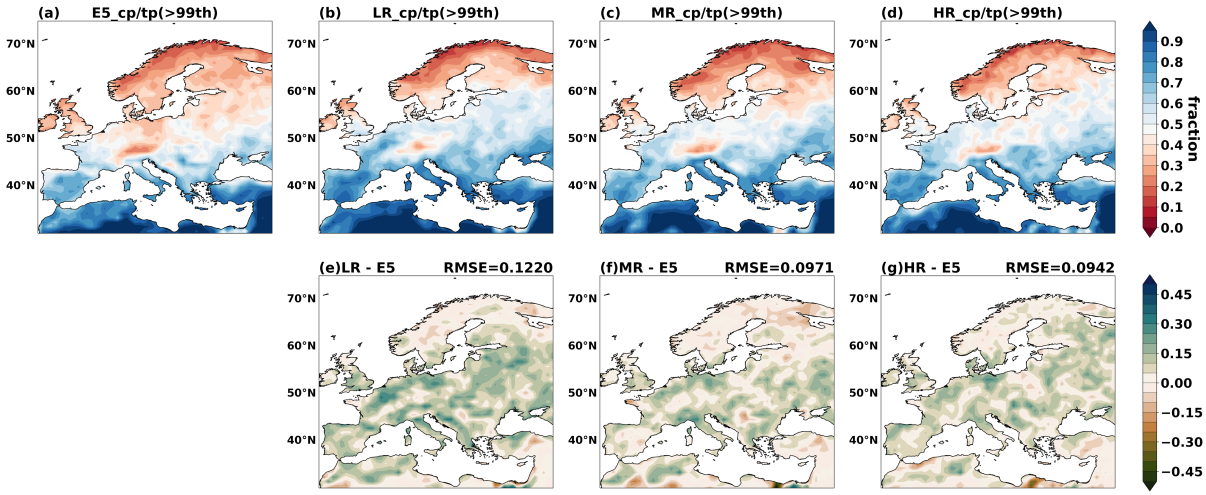

Fig. 4 Contribution of convective precipitation to extreme precipitation (>99th percentile) in (a) ERA5, (b) LR, (c) MR and (d) HR over Europe in JJA, and (e)– (g) their biases and RMSEs compared to ERA5 over the period 1982-2019.

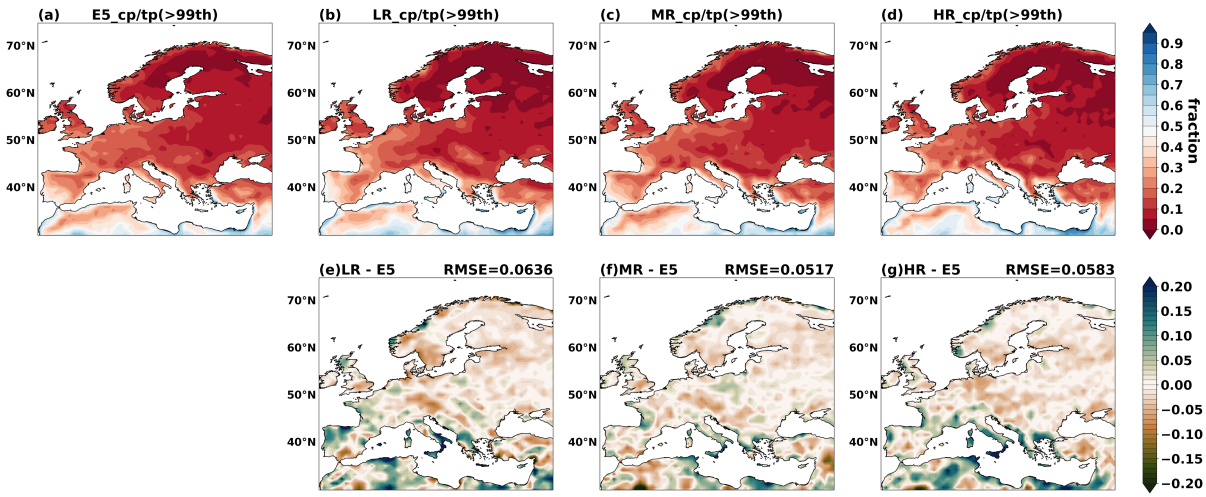

Fig. 5 The same as Fig. 4 but for DJF.

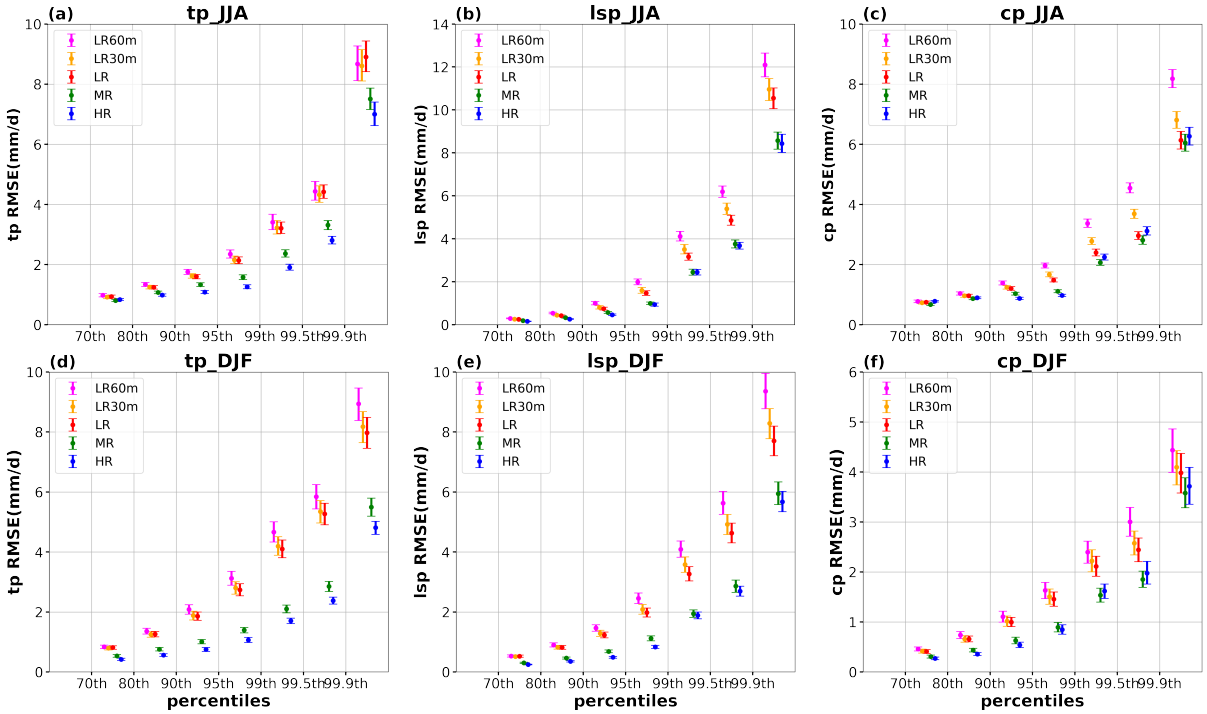

Fig. 6 RMSEs of total precipitation (a & d) at different percentile ranges (70th – 80th, 80th – 90th, 90th – 95th, 95th – 99th, 99th – 99.5th, 99.5th – 99.9th and >99.9th) and the corresponding large-scale precipitation (b & e) and convective precipitation (c & f) in OpenIFS simulations (LR60m: magenta, LR30m: orange, LR: red, MR: green, HR: blue) against ERA5 over Europe during 1982-2019. (a) – (c) are for JJA, and (d) – (f) for DJF. Dots are the RMSE values, and error bars are the 95 % confidence intervals. Unit is mm/d.

Table

Table 1: The experiment details of different horizontal resolutions and model time steps in OpenIFS.

	LR60m	LR30m	LR	MR	HR
Vertical resolution	L91			L91	L91
Horizontal Resolution	100 km (Tco95)			50 km (Tco199)	25 km (Tco399)
Time steps	60 minutes	30 minutes	15 minutes	15 minutes	15 minutes